

Task-Aware Resolution Optimization for Visual Large Language Models

Anonymous ACL submission

Abstract

Real-world vision-language applications demand varying levels of perceptual granularity. However, most existing visual large language models (VLLMs), such as LLaVA, pre-assume a fixed resolution for downstream tasks, which leads to subpar performance. To address this problem, we *first* conduct a comprehensive and pioneering investigation into the resolution preferences of different vision-language tasks, revealing a correlation between resolution preferences with ❶ image complexity, and ❷ uncertainty variance of the VLLM at different image input resolutions. Building on this insight, we propose an empirical formula to determine the optimal resolution for a given vision-language task, accounting for these two factors as the zeroth-order and first-order terms in the Taylor expansion on a given image input. *Second*, based on rigorous experiments, we propose a novel parameter-efficient fine-tuning technique to extend the visual input resolution of pre-trained VLLMs to the identified optimal resolution. Extensive experiments on various vision-language tasks validate the effectiveness of our method.

1 Introduction

Visual Large Language Models (VLLMs) represent a powerful class of models capable of handling vision-language tasks (Yin et al., 2023; Liu et al., 2023a, 2024; Alayrac et al., 2022). There is a growing body of research focused on the application of VLLMs in real-world scenarios, where different tasks necessitate varying levels of perceptual granularity. For instance, autonomous driving systems require high resolution to capture multiple objects and intricate details (Zhou et al., 2023; Ding et al., 2023), whereas image classification tasks involving singular, simple objects can be effectively performed at lower resolutions (Li et al., 2024a, 2023d; Zhang et al., 2024). Despite this, most existing VLLMs, *e.g.*, LLaVA, pre-assume a

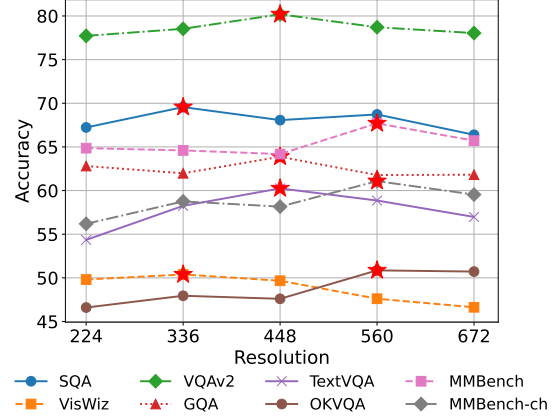


Figure 1: Resolution preference across eight tasks; ★ marks the optimal resolution for each task.

fixed resolution for downstream tasks, which leads to sub-optimal performance (Liu et al., 2023b,a; Li et al., 2023b). A direct “*exhaustive training*” strategy to adapt current VLLMs for diverse vision-language applications by training the models at different resolutions during the pre-training phase to create a series of checkpoints corresponding to various image input resolutions, followed by the selection of the most effective checkpoint for downstream tasks. While this method is viable, it incurs significant training costs. Consequently, we pose the first research question (**RQ1**):

RQ1: For a given vision-language task, how to accurately determine the optimal resolution without such exhaustive training for VLLMs?

To answer **RQ1**, we conduct a comprehensive and pioneering investigation into the resolution preferences across eight widely-studied vision-language tasks, utilizing VLLMs with five varying input image resolutions, as shown in Figure 1. Our findings reveal that directly choosing the lowest (224^2) and highest (672^2) resolution leads to subpar performance across tasks. On the other hand, we observe diverse preferences for the intermediate resolutions, with optimal choices scattered among 336^2 , 448^2 , and 560^2 .

To determine the resolution preference for different tasks, we propose two heuristic methods:

- ❶ image complexity, which measures the intrinsic complexity of a given image [❖ Section 3.2.1].
- ❷ uncertainty variance, which measures the variance of uncertainty in the model predictions at different image input resolutions [❖ Section 3.2.2].

These two heuristic methods can be regarded as the zeroth-order and the first-order terms in the Taylor expansion over image inputs [❖ Section 3.2.3]. Through empirical analysis across eight vision-language tasks, we find that both the complexity scores and model uncertainty variance exhibit a generally positive correlation with the preferred resolution for each task. Building on this insight, we propose an empirical formula integrating both heuristics to determine the optimal resolution for each vision-language task. We utilize three reference tasks to optimize a single hyperparameter of this empirical formula, and the fitting results across five additional tasks affirm its generalizability.

Once the optimal resolution for a given vision-language task is identified, the next step is adapting the current VLLM to the identified resolution. While the training-free method exists for resolution extension, we empirically find it would lead to performance degradation, suggesting that training-based approaches are essential. However, re-training a VLLM with another resolution from scratch incurs significant costs. This prompts our second research question (**RQ2**):

RQ2: *How to efficiently adapt a pre-trained VLLM to the designated resolution without compromise on the performance?*

To tackle this problem, we propose a post-training strategy that extends the image input resolution of an existing VLLM checkpoint. We conduct a preliminary experiment to identify which parameters within the VLLM are crucial for performance enhancement. Based on the findings, we propose a parameter-efficient fine-tuning (PEFT) approach, which only requires updating a few parameters in each VLLM component: the positional embedding parameters of the visual encoder, the projector parameters, and the LoRA adapter parameters of the LLM backbone. Empirical studies show that our method achieves the best efficiency-performance *Pareto front*. In summary, this paper has the following contributions:

- **Novel Discovery.** Through a comprehensive and pioneering investigation, we discover that differ-

ent vision-language tasks prefer distinct resolutions.

- **Empirical Formula.** We find these preferences correlated with image complexity and model uncertainty variance on samples at different input image resolutions, which can be interpreted as two terms in a Taylor Expansion of image inputs. We then propose an empirical formula to adaptively determine the optimal resolution for various downstream vision-language tasks without exhaustively training VLLMs.
- **Efficient Adaptation.** We introduce a PEFT approach to extend the input image resolution of LLaVA through post-training, containing three components, including vision module PEFT, language module PEFT, and the projector tuning.

2 Related Work

Vision Large Language Models (VLLMs). Vision Large Language Models (VLLMs) extend the capabilities of Large Language Models (LLMs) to multimodal tasks, enabling them to process both text and visual inputs (Alayrac et al., 2022; Liu et al., 2023a). This work focuses on VLLMs based on encoder-decoder architectures with modality connectors.

Dynamic Resolution in VLLMs. Dynamic resolution handling has become an important aspect of VLLMs, particularly for tasks involving images of varying sizes and aspect ratios. Models like Qwen2VL (Wang et al., 2024), MiniCPM (Yao et al., 2024), and LLaVA-UHD (Guo et al., 2025) have introduced strategies for processing high-resolution images dynamically. Unlike these methods, which often require architecture changes and from-scratch training, our approach uses a lightweight post-training strategy to adapt existing VLLM checkpoints for varying image resolutions.

Due to page limitations, more details are provided in Appendix A.

3 Methodology

This section elaborates on our proposed methodology. Section 3.1 presents an overview, followed by a detailed explanation of each component in Sections 3.2 and 3.3.

3.1 Method Framework

Figure 2 illustrates our approach, which consists of two key components. The first component fo-

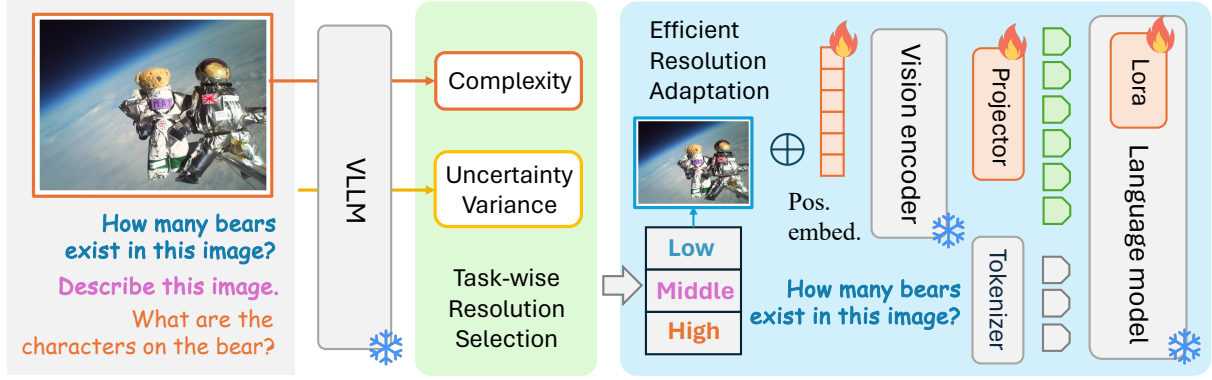


Figure 2: Our method comprises two components: the first component identifies the optimal image input resolution for a given vision-language task (depicted in green), while the second component adapts the VLLM to the selected image input resolution (depicted in blue).

cuses on task-specific resolution selection, where we introduce two heuristic approaches to determine the optimal resolution for a given vision-language task, detailed in Section 3.2.1 and 3.2.2. We explore the theoretical connection between these heuristics and the Taylor expansion on image input in Section 3.2.3, leading to an empirical formula that facilitates task-wise resolution selection in Section 3.2.4.

After identifying the optimal resolution, the second component adapts the VLLM to this specific resolution using a PEFT approach. This involves post-training a existing VLLM checkpoint without retraining the model from scratch. The PEFT adaptation process is discussed in detail in Section 3.3.

3.2 Task-wise Optimal Resolution Selection

As highlighted in Section 1, different vision-language tasks have varying requirements for the perceptual capacity of VLLMs. Therefore, it is critical to do task-wise resolution selection. While tuning VLLMs at different image input resolutions and obtaining the best-performing one is feasible, it imposes heavy training costs, which leads to *RQ1*. In this section, we propose a training-free method for determining the optimal resolution for a specific vision-language task, utilizing two heuristic approaches.

The first heuristic estimates the complexity of the images for each task, while the second evaluates the variance in model uncertainty at different input resolutions. We then derive an empirical formula to guide the resolution selection process.

3.2.1 Measuring Image Complexity

The initial step in VLLM processing is the perception of visual input. Intuitively, images with vary-

ing complexity levels demand different degrees of perceptual capacity, with more complex images requiring finer granularity in perception. Thus, for any given vision-language task, image complexity can serve as an indicator of resolution preference.

We propose to use Mahon and Lukasiewicz (2023) to measure image complexity, which applies hierarchical clustering on image pixels and leverages the minimum description length principle to determine the number of clusters. The average image complexity across samples of the specific task serves as an indicator for determining the appropriate resolution.

3.2.2 Measuring Uncertainty Variance across resolutions

In addition to the image complexity, which addresses only the visual aspects of a task, it is crucial to account for the model uncertainty of VLLMs, as it provides insights into the interaction between the visual and linguistic components of vision-language tasks. Furthermore, the method in Section 3.2.1 only captures static complexity, neglecting the effects of varying image resolutions. To complement this, we introduce the second heuristic approach based on model uncertainty.

Specifically, for a VLLM pre-trained at a fixed resolution (e.g., 336² for LLaVA), we extend the visual encoder’s resolution using position embedding interpolation, following methods employed in previous studies (Bai et al., 2023; Li et al., 2023b). We denote the original model as $M1$ and the extended-resolution model as $M2$. We first apply random augmentation to the images from the task, following the existing RandAugment algorithm (Cubuk et al., 2020). After augmentation, inference is conducted on the task samples using models $M1$ and

$M2$, from which we extract the softmax probabilities corresponding to each generated token. To quantify the uncertainty associated with each token, we calculate the information entropy using $H(p) = -\sum_{i=1}^n p_i \log p_i$. Here, $H(x)$ represents the entropy for token x , where $p(x_i)$ is the softmax probability of the i^{th} token and n is the number of possible tokens in the vocabulary. We denote the entropy values derived from $M1$ and $M2$ as $U1$ and $U2$, respectively, which provide a measure of uncertainty in the model’s predictions.

The uncertainty variance is computed as the ratio of the difference between $U1$ and $U2$ to $U1$, as shown in $r = \frac{U2-U1}{U1}$. Here, $V(T)$ represents the uncertainty variance for task T . This ratio quantifies how much the uncertainty changes between the two VLLMs, with higher values indicating a greater impact of resolution on the model’s uncertainty. This ratio is averaged across all generated tokens for a given sample, and the final uncertainty variance is computed by averaging this ratio across all samples in the task.

This heuristic approach serves two functions: (1) it computes entropy based on the tokens generated by VLLM, thus accounting for both visual and linguistic features during inference; and (2) it quantifies the variance caused by resolution changes, thereby capturing the dynamic effects of resolution shifts. Unlike the static image complexity heuristic, this method emphasizes the impact of resolution modifications, making these two heuristics complementary.

Notably, we extend the image input resolution of VLLM without tuning the model parameters, allowing us to avoid additional training costs.

3.2.3 Designing Heuristic from the Taylor Expansion Perspective

We further interpret the two heuristics using a Taylor expansion perspective on image inputs. As shown in Equation 1, the Taylor expansion is defined over image inputs, where I represents an image, R denotes its resolution, and $F(I, R)$ represents the overall model evaluation. $C(I)$ denotes the image complexity, which captures the intrinsic properties of the image, while $V(I)$ represents the uncertainty variance, indicating the model’s sensitivity to changes in resolution. ΔR refers to the difference between two resolutions, and $H(I, R)$ represents higher-order terms related to resolution

changes.

$$F(I, R) = C(I) + V(I) \cdot \Delta R + \frac{H(I, R)}{2!} (\Delta R)^2 + \dots \quad (1)$$

In the simplified form shown in Equation 2, only the zeroth-order and the first-order terms are considered:

$$F(I, R) \approx C(I) + V(I) \cdot \Delta R \quad (2)$$

This simplified expression highlights the inherent complexity of the image ($C(I)$) and the linear change in model uncertainty due to resolution variations ($V(I) \cdot \Delta R$). This framework underlines the importance of accounting for both the intrinsic properties of images and the model’s response to resolution changes.

3.2.4 Empirical Formula

Intuitively, tasks characterized by high image complexity often necessitate higher input resolutions. Similarly, tasks with high uncertainty variance indicate that increasing resolution heightens model uncertainty, which suggests a need for greater perceptual capacity. Conversely, low uncertainty variance suggests that resolution changes exert minimal impact, making higher resolutions unnecessary. Based on these observations, we hypothesize that image complexity and uncertainty variance are positively correlated with the preferred resolution. Consequently, we propose Equation 3 to determine the optimal resolution for a specific vision-language task T :

$$Reso(T) = Reso_0(1 + k \times C(T) \times V(T)) \quad (3)$$

In this empirical formula, $C(T)$ represents the averaged normalized image complexity for task T , $V(T)$ denotes the averaged uncertainty variance across different image input resolutions on task T , k is a user-specified hyperparameter, and $Reso_0$ is the baseline image input resolution of the original VLLM. The expression $1 + k \times C(T) \times V(T)$ quantifies the scaling factor between the baseline and the preferred resolution. In practice, the value of k can be adjusted based on prior experience.

3.3 Parameter-efficient Resolution Adaptation

After determining the optimal resolution for a given task, the next step is adapting the VLLM to the selected resolution. To answer **RQ2**, We propose a parameter-efficient fine-tuning (PEFT) approach

Table 1: A comprehensive investigation conducted to explore resolution preferences across eight vision-language tasks. For each task, the accuracy scores corresponding to five different resolutions are presented.

Resolution	SciQA-IMG	VizWiz	VQAv2	GQA	TextVQA	OKVQA	MMBench	MMBench-CN
224×224	67.23	49.81	77.72	62.81	54.35	46.60	64.86	56.19
336×336	69.56	50.39	78.53	61.98	58.25	47.95	64.60	58.76
448×448	68.07	49.67	80.19	63.87	60.25	47.60	64.18	58.16
560×560	68.72	47.61	78.71	61.77	58.86	50.86	67.70	61.08
672×672	66.39	46.63	78.04	61.82	56.98	50.72	65.72	59.54

that post-train an existing VLLM checkpoint, thus avoiding retraining from scratch.

As depicted in Figure 2, existing VLLMs (e.g., LLaVA) consist of three main components: a visual encoder that processes visual inputs, a projector that maps visual features to the word embedding space, and an LLM backbone that autoregressively generates language tokens based on the combined visual and linguistic inputs.

Increasing the input resolution results in more image patches, which introduces incompatibility with the original position embeddings. To address this, we interpolate the position embeddings from the initial number of patches (e.g., 24^2) to the extended number (e.g., 32^2), following previous research (Bai et al., 2023; Li et al., 2023b). Although this allows the VLLM to process extended resolutions, performance degrades without further adaptation (as discussed in Section 3.2). To counter this performance decline, we employ a PEFT method that fine-tunes three key components: (1) position embeddings within the visual encoder, crucial for resolution adaptation due to the change in image patch count; (2) the lightweight projector parameters; and (3) the parameters of the LoRA adapters integrated into the LLM backbone. By keeping all other parameters frozen, the PEFT approach offers an efficient method for adaptation. Figure 2 provides a visual representation of the components that are fine-tuned versus those that remain frozen.

4 Experiments

This section presents the empirical evaluation of our proposed method. We first introduce the implementation details in Section 4.1, followed by an in-depth analysis of the results, including the investigation into resolution preferences, task-wise resolution selection, and the findings from the ablation study in Section 4.2, Section 4.3, and Section 4.4, respectively.

4.1 Implementation Details

VLLM Selection. For our experiments, we select the LLaVA-1.5-7B checkpoint (Liu et al., 2023b) as the representative VLLM for evaluation.

Resolution Configurations. We explore five image resolutions: 224^2 , 336^2 , 448^2 , 560^2 , and 672^2 . These values cover the resolution spectrum commonly used in previous studies (Liu et al., 2023b,a).

Vision-Language Tasks. Our evaluation encompasses eight vision-language tasks, with details introduced in Appendix B.1.

Baseline Methods. In addition to the original LLaVA model, we compare our method with several state-of-the-art approaches. Besides, we report the performance of position embedding interpolation as a representative of the training-free methods to extend the image input resolution of VLLMs. The details are introduced in Appendix B.2.

Post-training Details. To initialize the position embedding parameters of the visual encoder (Vision Transformer) in LLaVA during resolution adaptation, we employ extended position embeddings derived through positional embedding interpolation, as described in Appendix B.2. Following the post-training instructions provided by the LLaVA authors¹, we concentrate on stage 2 fine-tuning, incorporating the additional parameters for position embeddings in the visual encoder, alongside the LoRA adapter and projector parameters. The fine-tuning process utilizes images from five datasets: COCO (Lin et al., 2014), GQA (Hudson and Manning, 2019), OCR-VQA (Mishra et al., 2019), TextVQA (Singh et al., 2019), and Visual Genome (Krishna et al., 2017). For more details on the construction of the image-text pairs used in training, we refer readers to (Liu et al., 2023a).

More details about method implementation and PEFT are introduced in Appendix B.3 and B.4.

¹<https://github.com/haotian-liu/LLaVA/tree/main?tab=readme-ov-file#train>

Table 2: Distributions of image complexity and uncertainty variance across eight tasks.

	vizwiz	SciQA-IMG	TextVQA	GQA	VQAv2	OKVQA	MMBench	MMBench-CN
Resolution Preference	336 × 336		448 × 448			560 × 560		
Complexity (C)	0.2191	0.1437	0.2919	0.3236	0.3017	0.3112	0.2323	0.2329
Average	0.1814		0.3058			0.2588		
Uncertainty Variance (V)	1.83%	6.47%	4.88%	5.34%	5.26%	6.72%	10.79%	10.45%
Average	4.15%		5.16%			9.32%		
C × V	0.0040	0.0093	0.0142	0.0173	0.0159	0.0209	0.0251	0.0243
Average	0.0067		0.0158			0.0234		

Table 3: Comparison between our method and baseline approaches, highlighting the best scores in bold. * indicates that the training images or annotations of the datasets were observed during training.

Method	LLM	Resolution	Post-training	VQAv2	GQA	TextVQA	OKVQA	MMBench	MMBench-CN
BLIP-2	Vicuna-13B	224 × 224	-	65.00	41.00	42.50	-	-	-
InstructBLIP	Vicuna-7B	224 × 224	-	-	49.20	50.10	-	36.00	23.70
InstructBLIP	Vicuna-13B	224 × 224	-	-	49.50	50.70	-	-	-
Shikra	Vicuna-13B	224 × 224	-	77.40*	-	-	-	58.80	-
IDEFICS-9B	LLaMA-7B	224 × 224	-	50.90	38.40	25.90	-	48.20	25.20
IDEFICS-80B	LLaMA-65B	224 × 224	-	60.00	45.20	30.90	-	54.50	38.10
Qwen-VL	Qwen-7B	448 × 448	-	78.80*	59.30*	63.80*	-	38.20	7.40
Qwen-VL-Chat	Qwen-7B	448 × 448	-	78.20*	57.50*	61.50*	-	60.60	56.70
LLaVA-1.5	Vicuna-7B	336 × 336	-	78.53*	61.98*	58.25	47.95	64.60	58.76
LLaVA-1.5	Vicuna-7B	448 × 448	✗	77.82*	61.29*	56.61	47.38	63.32	57.73
LLaVA-1.5	Vicuna-7B	448 × 448	✓	80.19*	63.87*	60.25	47.60	64.18	58.16
LLaVA-1.5	Vicuna-7B	560 × 560	✓	78.71*	61.77*	58.86	50.86	67.70	61.08
LLaVA-1.5	Vicuna-7B	Adaptive	✓	80.19*	63.87*	60.25	50.86	67.70	61.08
LLaVA-1.5	Vicuna-13B	336 × 336	-	80.00*	63.30*	61.30	-	67.70	63.60

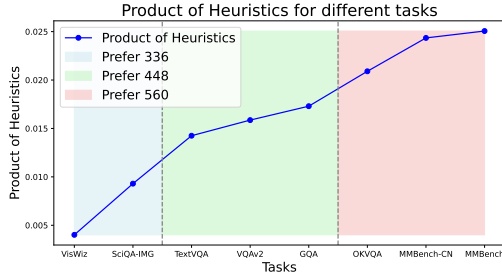


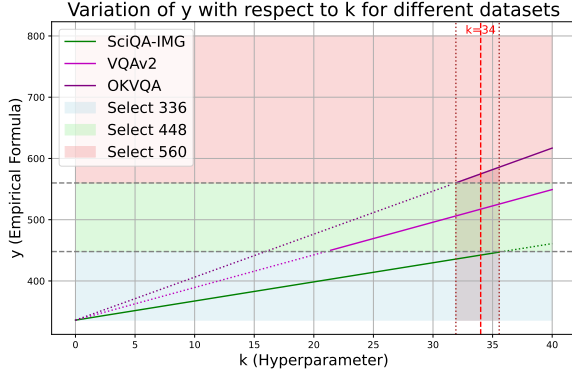
Figure 3: The product of two heuristic scores exhibits a consistent correlation with resolution preferences.

4.2 Analyzing Resolution Preferences Across Vision-Language Tasks

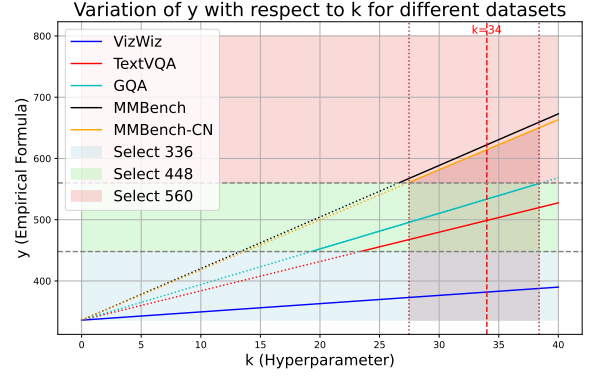
We conduct a comprehensive empirical study to analyze the resolution preferences across various vision-language tasks systematically, summarized in Table 1. The findings reveal two key observations: ❶ Performance is suboptimal when image resolution is either too low (224^2) or too high (672^2): low resolution limits the model’s ability to capture visual details, while high resolution creates a gap between the original and extended input, leading to ineffective adaptation and excess irrelevant tokens. ❷ Optimal resolutions are found at intermediate values (336^2 , 448^2 , 560^2), indicating that

each task has different granularity needs. No fixed resolution works best for all tasks, highlighting the importance of task-specific resolution selection.

After identifying task-specific resolution preferences, we explore the correlation between optimal resolutions and our proposed heuristics of image complexity and uncertainty variance, as shown in Table 2. We can draw the following conclusions: ❶ No increasing trend is observed between 448^2 and 560^2 in image complexity, but a noticeable gap exists between 336^2 and 448^2 , suggesting that image complexity differentiates tasks favoring 336^2 from those preferring higher resolutions. ❷ There is a positive correlation between preferred resolution and uncertainty variance across tasks, with an upward trend showing that uncertainty variance reliably indicates resolution preference. ❸ Some exceptions exist, e.g., GQA prefers lower resolution than MMBench but has higher image complexity, and SciQA-IMG has higher uncertainty variance but favors a lower resolution than TextVQA. Combining both heuristics (by multiplying their scores) provides a more consistent correlation, as shown in Figure 3.



(a) Optimization of the hyperparameters in the empirical formula using three reference tasks.



(b) The empirical formula demonstrates effective generalization across five vision-language tasks.

Figure 4: Applying the empirical formula to determine the optimal resolution for vision-language tasks.

4.3 Evaluating Heuristic-Based Task-Specific Resolution Selection

The investigation presents the correlation between task-specific resolution preferences and two heuristic approaches, especially when their scores are combined. In this section, we describe how the hyperparameter values are determined in the empirical formula and summarize the performance of models using this strategy.

4.3.1 Applying the empirical formula to determine the optimal resolution

To optimize the hyperparameter in Equation 3, we select three reference tasks representing different visual perception requirements (Figure 6 in Appendix D shows task images). Tasks with simpler images (e.g., Figure 6a) are considered low resolution, while complex images (e.g., Figure 6c) require higher resolutions. Intermediate tasks (e.g., Figure 6b) represent medium resolution. SciQA-IMG, VQAv2, and OKVQA are separately chosen to reflect low, medium, and high resolution needs.

When tuning the hyperparameter k , we focus on 336^2 , 448^2 , and 560^2 . The constant Res_{00} is set to 336 (default LLaVA resolution). The formula selects the resolution based on the value of k . For example, a value of 500 leads to 448^2 .

Figure 4a visualizes the relationship between hyperparameter values and selected resolutions. For simplicity, we select $k = 34$, which results in optimal resolution selection for the reference tasks. Additionally, as shown in Figure 4b, this value generalizes well to other tasks, achieving the best resolution for each.

So far, we have utilized the mean value of image complexity and uncertainty variance to characterize

the specific task. In Appendix C, we analyze the sample-level distributions of image complexity and uncertainty variance, as well as their impact on the empirical formula performance.

4.3.2 Overall results of Task-wise Adaptive Model and Baselines

Table 3 presents the performance of baseline methods and LLaVA variants across six tasks that demand high visual perception capacity from VLLMs. Among the LLaVA variants, the training-free method to extend the input resolution through PE interpolation shows performance degradation at varying levels. This confirms that the position embeddings in the visual encoder and LLM backbone in LLaVA cannot fully adapt to the increased number of image tokens without post-training. On the other hand, the task-wise adaptive LLaVA variant, which optimally selects the input resolution for each task, achieves the best overall performance compared to fixed-resolution LLaVA variants, regardless of whether the resolution is 336^2 , 448^2 , or 560^2 . Notably, the task-wise adaptive LLaVA variant with a 7B backbone performs comparably to the 13B variant, underscoring the importance of adaptive perception capacity in VLLMs.

When comparing the task-wise adaptive LLaVA variant with other state-of-the-art baselines, it outperforms all but the TextVQA task. In the case of TextVQA, the Qwen-VL and Qwen-VL-Chat methods have observed training images or annotations of the dataset during their training. Importantly, as previous studies (McKinzie et al., 2024a) have highlighted, resolution plays a crucial role during pretraining. The Qwen-VL series are pretrained at an image resolution of 448^2 , while the LLaVA vari-

Resolution	ViT PE	Projector	LoRA Adapter	VQAv2	GQA	TextVQA
336 × 336	-	-	-	78.53	61.98	58.25
448 × 448	✗	✗	✗	77.82	61.29	56.61
448 × 448	✓	✗	✗	75.32	59.98	53.44
448 × 448	✗	✓	✗	72.94	55.31	51.41
448 × 448	✗	✓	✓	79.47	63.41	58.06
448 × 448	✓	✓	✓	80.19	63.87	60.25

Table 4: Ablation Analysis of PEFT Components, ✗ and ✓ indicate whether the module is post-trained.

ants were fine-tuned at extended image resolutions in a post-training phase with far fewer data (665K) compared to Qwen’s 1.4B pretraining and 50M fine-tuning samples. Nevertheless, the task-wise adaptive LLaVA variant achieves better overall results than the Qwen-VL series.

The superior performance of the task-wise adaptive LLaVA variant across multiple vision-language tasks demonstrates that, compared to *fixed-resolution* approaches, *adaptive resolution selection* is more suitable for real-world applications. So far, we have verified the effectiveness of our proposed task-wise resolution selection strategy through the generalization of the empirical formula and the overall experimental results, answering **RQ1**.

4.4 Ablation Analysis of PEFT Components for Performance

To evaluate the contribution of each component in our proposed PEFT method, we perform an ablation study, as shown in Table 4. Specifically, we examine the impact of tuning three components of parameters: the position embeddings within the visual encoder, the LoRA adapters in the LLM backbone, and the projector parameters.

The results indicate that tuning each component is crucial for achieving optimal performance. When tuning only the position embeddings or projector parameters, we observe a substantial degradation in performance, even compared to the training-free approach utilizing positional embedding interpolation. While the combined tuning of projector parameters and LoRA adapters yields noticeable improvements, the performance remains suboptimal without concurrent tuning of the position embeddings. These findings highlight the essential role of each component in the PEFT method. So far, through the overall experimental results and the ablation experimental analysis of each component in our proposed PEFT method, we verified the effectiveness of our proposed PEFT method, answering **RQ2**.

5 Case Study

As summarized in Appendix E, we present two case studies illustrating the impact of image complexity and uncertainty variance on VLLM performance.

Table 8 compares the performance of a VLLM when presented with two images of differing complexity levels, as measured by our method. Both images are associated with the same question, which asks the model to identify "who is standing." For the image with lower complexity (Figure 7a), the VLLM at a resolution of 336² correctly identifies the woman standing. Conversely, for the image characterized by a more intricate background (Figure 7b), the model fails to provide the correct identification. This outcome indicates that an increased image input resolution is essential for effectively processing more visually complex images.

Table 9 examines a scenario where the same image is used to answer two questions of differing difficulty. The image shows a room’s interior. For the easier question about the material of a sheet, the VLLM at 336² resolution provides a correct answer. However, for the more complex question about the location of a smaller object (a tap), the model fails at 336² but succeeds at 448², highlighting improved performance with higher resolution. Uncertainty variance is low for the simpler question but significantly higher for the complex one, supporting the hypothesis in Section 3.2.4.

6 Conclusion

In this paper, we take a step towards adapting VLLMs to real-world applications by providing an in-depth investigation of resolution preferences in different vision-language tasks. Based on the findings, we introduce an empirical formula that combines image complexity and uncertainty variance to make task-specific resolution selection without the need for retraining. Additionally, we propose a PEFT approach, enabling extension of the image input resolution for existing VLLM checkpoints. We expect that our research will offer valuable insights for the VLLM research community.

Limitations & Future Work

Our current work has several limitations. Due to computational constraints in an academic environment, we were unable to conduct experiments with larger LLM backbones or retrain models from scratch. This restricts the scope of comparison, particularly against methods requiring extensive per-training. Moreover, our proposed approach focuses on task-level resolution selection. Future work will explore more granular resolution strategies, such as dynamic sample-level resolution adaptation, which could further improve performance for heterogeneous tasks.

Ethical Statement

This study leverages publicly available datasets (e.g., VQA_{v2}, GQA, TextVQA, OKVQA, MM-Bench) and pre-trained models (e.g., LLaVA) for evaluation and experimentation. These datasets and models are widely recognized benchmarks in the vision-language research community, distributed under licenses permitting academic and non-commercial use. All artifacts were used in accordance with their intended purposes, without modifications or new data collection. The dataset creators' documentation ensures compliance with ethical guidelines, including the absence of personally identifiable or offensive content.

No ethics review board approval was required, as this research does not involve human subject data or sensitive information. However, we acknowledge that the underlying datasets may contain biases or inaccuracies, which could affect model fairness and generalization. Future research should explore bias mitigation strategies to ensure fair and responsible deployment of vision-language models. The derivative findings, such as task-specific resolution adaptation strategies, remain compatible with the original licenses and intended use.

References

[Fuyu-8b: A multimodal architecture for ai agents.](#)

Jean-Baptiste Alayrac, Jeff Donahue, Pauline Luc, Antoine Miech, Iain Barr, Yana Hasson, Karel Lenc, Arthur Mensch, Katie Millican, Malcolm Reynolds, Roman Ring, Eliza Rutherford, Serkan Cabi, Tengda Han, Zhitao Gong, Sina Samangooei, Marianne Monteiro, Jacob Menick, Sebastian Borgeaud, Andy Brock, Aida Nematzadeh, Sahand Sharifzadeh, Mikołaj Binkowski, Ricardo Barreira, Oriol Vinyals, Andrew Zisserman, and Karen Simonyan. 2022.

Flamingo: a visual language model for few-shot learning. *ArXiv*, abs/2204.14198.

Anas Awadalla, Irena Gao, Josh Gardner, Jack Hessel, Yusuf Hanafy, Wanrong Zhu, Kalyani Marathe, Yonatan Bitton, Samir Yitzhak Gadre, Shiori Sagawa, Jenia Jitsev, Simon Kornblith, Pang Wei Koh, Gabriel Ilharco, Mitchell Wortsman, and Ludwig Schmidt. 2023. Openflamingo: An open-source framework for training large autoregressive vision-language models. *ArXiv*, abs/2308.01390.

Jinze Bai, Shuai Bai, Shusheng Yang, Shijie Wang, Sinan Tan, Peng Wang, Junyang Lin, Chang Zhou, and Jingren Zhou. 2023. Qwen-vl: A frontier large vision-language model with versatile abilities. *arXiv preprint arXiv:2308.12966*.

Keqin Chen, Zhao Zhang, Weili Zeng, Richong Zhang, Feng Zhu, and Rui Zhao. 2023. Shikra: Unleashing multimodal llm's referential dialogue magic. *arXiv preprint arXiv:2306.15195*.

Ekin D Cubuk, Barret Zoph, Jonathon Shlens, and Quoc V Le. 2020. Randaugment: Practical automated data augmentation with a reduced search space. In *Proceedings of the IEEE/CVF conference on computer vision and pattern recognition workshops*, pages 702–703.

Wenliang Dai, Nayeon Lee, Boxin Wang, Zhuoling Yang, Zihan Liu, Jon Barker, Tuomas Rintamäki, Mohammad Shoeybi, Bryan Catanzaro, and Wei Ping. 2024. [NVLM: Open Frontier-Class Multimodal LLMs](#). *arXiv e-prints*, arXiv:2409.11402.

Wenliang Dai, Junnan Li, Dongxu Li, Anthony Meng Huat Tiong, Junqi Zhao, Weisheng Wang, Boyang Li, Pascale Fung, and Steven Hoi. 2024. Instructblip: towards general-purpose vision-language models with instruction tuning. In *Proceedings of the 37th International Conference on Neural Information Processing Systems*, NIPS '23, Red Hook, NY, USA. Curran Associates Inc.

Jia Deng, Wei Dong, Richard Socher, Li-Jia Li, Kai Li, and Li Fei-Fei. 2009. Imagenet: A large-scale hierarchical image database. In *2009 IEEE conference on computer vision and pattern recognition*, pages 248–255. Ieee.

Xinpeng Ding, Jianhua Han, Hang Xu, Wei Zhang, and X. Li. 2023. Hilm-d: Towards high-resolution understanding in multimodal large language models for autonomous driving. *ArXiv*, abs/2309.05186.

Danny Driess, F. Xia, Mehdi S. M. Sajjadi, Corey Lynch, Aakanksha Chowdhery, Brian Ichter, Ayzaan Wahid, Jonathan Tompson, Quan Ho Vuong, Tianhe Yu, Wenlong Huang, Yevgen Chebotar, Pierre Sermanet, Daniel Duckworth, Sergey Levine, Vincent Vanhoucke, Karol Hausman, Marc Toussaint, Klaus Greff, Andy Zeng, Igor Mordatch, and Peter R. Florence. 2023. Palm-e: An embodied multimodal language model. In *International Conference on Machine Learning*.

Hao Feng, Qi Liu, Hao Liu, Wen gang Zhou, Houqiang Li, and Can Huang. 2023. Docpedia: Unleashing the power of large multimodal model in the frequency domain for versatile document understanding. <i>ArXiv</i> , abs/2311.11810.	762
Yash Goyal, Tejas Khot, Douglas Summers-Stay, Dhruv Batra, and Devi Parikh. 2017. Making the v in vqa matter: Elevating the role of image understanding in visual question answering. In <i>Proceedings of the IEEE conference on computer vision and pattern recognition</i> , pages 6904–6913.	763
Zonghao Guo, Ruyi Xu, Yuan Yao, Junbo Cui, Zanolin Ni, Chunjiang Ge, Tat-Seng Chua, Zhiyuan Liu, and Gao Huang. 2025. Llava-uhd: an lmm perceiving any aspect ratio and high-resolution images. In <i>European Conference on Computer Vision</i> , pages 390–406. Springer.	764
Danna Gurari, Qing Li, Abigale J Stangl, Anhong Guo, Chi Lin, Kristen Grauman, Jiebo Luo, and Jeffrey P Bigham. 2018. Vizwiz grand challenge: Answering visual questions from blind people. In <i>Proceedings of the IEEE conference on computer vision and pattern recognition</i> , pages 3608–3617.	765
Wenyi Hong, Weihang Wang, Qingsong Lv, Jiazheng Xu, Wenmeng Yu, Junhui Ji, Yan Wang, Zihan Wang, Yuxiao Dong, Ming Ding, and Jie Tang. 2023. Cogagent: A visual language model for gui agents. <i>2024 IEEE/CVF Conference on Computer Vision and Pattern Recognition (CVPR)</i> , pages 14281–14290.	766
Anwen Hu, Haiyang Xu, Jiabo Ye, Mingshi Yan, Liang Zhang, Bo Zhang, Chen Li, Ji Zhang, Qin Jin, Fei Huang, and Jingren Zhou. 2024. mplug-docowl 1.5: Unified structure learning for ocr-free document understanding. <i>ArXiv</i> , abs/2403.12895.	767
Drew A Hudson and Christopher D Manning. 2019. Gqa: A new dataset for real-world visual reasoning and compositional question answering. In <i>Proceedings of the IEEE/CVF conference on computer vision and pattern recognition</i> , pages 6700–6709.	768
IDEFICS. 2023. Introducing idefics: An open reproduction of state-of-the-art visual language model. https://huggingface.co/blog/idefics .	769
Ranjay Krishna, Yuke Zhu, Oliver Groth, Justin Johnson, Kenji Hata, Joshua Kravitz, Stephanie Chen, Yannis Kalantidis, Li-Jia Li, David A Shamma, et al. 2017. Visual genome: Connecting language and vision using crowdsourced dense image annotations. <i>International journal of computer vision</i> , 123:32–73.	770
Bo Li, Yuanhan Zhang, Liangyu Chen, Jinghao Wang, Jingkang Yang, and Ziwei Liu. 2023a. Otter: A multi-modal model with in-context instruction tuning. <i>ArXiv</i> , abs/2305.03726.	771
Junnan Li, Dongxu Li, Silvio Savarese, and Steven Hoi. 2023b. Blip-2: Bootstrapping language-image pre-training with frozen image encoders and large language models. In <i>International conference on machine learning</i> , pages 19730–19742. PMLR.	772
Junyan Li, Delin Chen, Tianle Cai, Peihao Chen, Yining Hong, Zhenfang Chen, Yikang Shen, and Chuang Gan. 2024a. Flexattention for efficient high-resolution vision-language models. <i>ArXiv</i> , abs/2407.20228.	773
Yanwei Li, Yuechen Zhang, Chengyao Wang, Zhisheng Zhong, Yixin Chen, Ruihang Chu, Shaoteng Liu, and Jiaya Jia. 2024b. Mini-gemini: Mining the potential of multi-modality vision language models. <i>ArXiv</i> , abs/2403.18814.	774
Zhang Li, Biao Yang, Qiang Liu, Zhiyin Ma, Shuo Zhang, Jingxu Yang, Yabo Sun, Yuliang Liu, and Xiang Bai. 2023d. Monkey: Image resolution and text label are important things for large multi-modal models. <i>2024 IEEE/CVF Conference on Computer Vision and Pattern Recognition (CVPR)</i> , pages 26753–26763.	775
Tsung-Yi Lin, Michael Maire, Serge Belongie, James Hays, Pietro Perona, Deva Ramanan, Piotr Dollár, and C Lawrence Zitnick. 2014. Microsoft coco: Common objects in context. In <i>Computer Vision—ECCV 2014: 13th European Conference, Zurich, Switzerland, September 6–12, 2014, Proceedings, Part V 13</i> , pages 740–755. Springer.	776
Haotian Liu, Chunyuan Li, Yuheng Li, and Yong Jae Lee. 2023a. Improved baselines with visual instruction tuning.	777
Haotian Liu, Chunyuan Li, Yuheng Li, Bo Li, Yuanhan Zhang, Sheng Shen, and Yong Jae Lee. 2024. <i>Llava-next: Improved reasoning, ocr, and world knowledge</i> .	778
Haotian Liu, Chunyuan Li, Qingyang Wu, and Yong Jae Lee. 2023b. Visual instruction tuning.	779
Yuan Liu, Haodong Duan, Yuanhan Zhang, Bo Li, Songyang Zhang, Wangbo Zhao, Yike Yuan, Jiaqi Wang, Conghui He, Ziwei Liu, et al. 2023c. Mmbench: Is your multi-modal model an all-around player? <i>arXiv preprint arXiv:2307.06281</i> .	780
Pan Lu, Swaroop Mishra, Tanglin Xia, Liang Qiu, Kai-Wei Chang, Song-Chun Zhu, Oyvind Tafjord, Peter Clark, and Ashwin Kalyan. 2022. Learn to explain: Multimodal reasoning via thought chains for science question answering. <i>Advances in Neural Information Processing Systems</i> , 35:2507–2521.	781
Tengchao Lv, Yupan Huang, Jingye Chen, Lei Cui, Shuming Ma, Ya-Chi Chang, Shaohan Huang, Wenhui Wang, Li Dong, Weiyao Luo, Shaoxiang Wu, Guoxin Wang, Cha Zhang, and Furu Wei. 2023. Kosmos-2.5: A multimodal literate model. <i>ArXiv</i> , abs/2309.11419.	782

816	Louis Mahon and Thomas Lukasiewicz. 2023. Minimum description length clustering to measure meaningful image complexity. <i>arXiv preprint arXiv:2306.14937</i> .	872
817		873
818		874
819		875
820	Kenneth Marino, Mohammad Rastegari, Ali Farhadi, and Roozbeh Mottaghi. 2019. Ok-vqa: A visual question answering benchmark requiring external knowledge. In <i>Proceedings of the IEEE/cvf conference on computer vision and pattern recognition</i> , pages 3195–3204.	876
821		877
822		
823		878
824		879
825		880
826		881
827	Brandon McKinzie, Zhe Gan, Jean-Philippe Fauconier, Sam Dodge, Bowen Zhang, Philipp Dufter, Dhruti Shah, Xianzhi Du, Futang Peng, Floris Weers, et al. 2024a. Mml: Methods, analysis & insights from multimodal llm pre-training. <i>arXiv preprint arXiv:2403.09611</i> .	882
828		
829		883
830		884
831		885
832		886
833	Brandon McKinzie, Zhe Gan, Jean-Philippe Fauconier, Sam Dodge, Bowen Zhang, Philipp Dufter, Dhruti Shah, Xianzhi Du, Futang Peng, Floris Weers, et al. 2024b. Mml: Methods, analysis & insights from multimodal llm pre-training. <i>arXiv preprint arXiv:2403.09611</i> .	887
834		888
835		889
836		890
837		891
838		892
839	Anand Mishra, Shashank Shekhar, Ajeet Kumar Singh, and Anirban Chakraborty. 2019. Ocr-vqa: Visual question answering by reading text in images. In <i>2019 international conference on document analysis and recognition (ICDAR)</i> , pages 947–952. IEEE.	893
840		894
841		895
842		896
843	Amanpreet Singh, Vivek Natarajan, Meet Shah, Yu Jiang, Xinlei Chen, Dhruv Batra, Devi Parikh, and Marcus Rohrbach. 2019. Towards vqa models that can read. In <i>Proceedings of the IEEE/CVF conference on computer vision and pattern recognition</i> , pages 8317–8326.	897
844		898
845		899
846		900
847		901
848		902
849	Chameleon Team. 2024. Chameleon: Mixed-modal early-fusion foundation models. <i>ArXiv</i> , abs/2405.09818.	903
850		904
851		905
852		906
853	Shengbang Tong, Ellis Brown, Penghao Wu, Sanghyun Woo, Manoj Middepogu, Sai Charitha Akula, Jihan Yang, Shusheng Yang, Adithya Iyer, Xichen Pan, et al. 2024. Cambrian-1: A fully open, vision-centric exploration of multimodal llms. <i>arXiv preprint arXiv:2406.16860</i> .	907
854		908
855		909
856		910
857		911
858		
859	Peng Wang, Shuai Bai, Sinan Tan, Shijie Wang, Zhihao Fan, Jinze Bai, Keqin Chen, Xuejing Liu, Jialin Wang, Wenbin Ge, et al. 2024. Qwen2-vl: Enhancing vision-language model’s perception of the world at any resolution. <i>arXiv preprint arXiv:2409.12191</i> .	912
860		
861		913
862		914
863		915
864	Haoran Wei, Lingyu Kong, Jinyue Chen, Liang Zhao, Zheng Ge, Jinrong Yang, Jian-Yuan Sun, Chunrui Han, and Xiangyu Zhang. 2023. Vary: Scaling up the vision vocabulary for large vision-language models. <i>ArXiv</i> , abs/2312.06109.	916
865		917
866		918
867		919
868		920
869	Xiao wen Dong, Pan Zhang, Yuhang Zang, Yuhang Cao, Bin Wang, Linke Ouyang, Songyang Zhang, Haodong Duan, Wenwei Zhang, Yining Li, Hang Yan, Yang Gao, Zhe Chen, Xinyue Zhang, Wei Li, Jingwen Li, Wenhai Wang, Kai Chen, Conghui He, Xingcheng Zhang, Jifeng Dai, Yuxin Qiao, Dahua Lin, and Jiaqi Wang. 2024. Internlm-xcomposer2-4khd: A pioneering large vision-language model handling resolutions from 336 pixels to 4k hd. <i>ArXiv</i> , abs/2404.06512.	921
870		922
871		923
		924
	Ruyi Xu, Yuan Yao, Zonghao Guo, Junbo Cui, Zanlin Ni, Chunjiang Ge, Tat-Seng Chua, Zhiyuan Liu, Maosong Sun, and Gao Huang. 2024. Llava-uhd: an lmm perceiving any aspect ratio and high-resolution images. <i>ArXiv</i> , abs/2403.11703.	
	Le Xue, Manli Shu, Anas Awadalla, Jun Wang, An Yan, Senthil Purushwalkam, Honglu Zhou, Viraj Prabhu, Yutong Dai, Michael S Ryoo, et al. 2024. xgen-mm (blip-3): A family of open large multimodal models. <i>arXiv preprint arXiv:2408.08872</i> .	
	Yuan Yao, Tianyu Yu, Ao Zhang, Chongyi Wang, Junbo Cui, Hongji Zhu, Tianchi Cai, Haoyu Li, Weilin Zhao, Zhihui He, et al. 2024. Minicpm-v: A gpt-4v level mllm on your phone. <i>arXiv preprint arXiv:2408.01800</i> .	
	Shukang Yin, Chaoyou Fu, Sirui Zhao, Ke Li, Xing Sun, Tong Xu, and Enhong Chen. 2023. A survey on multimodal large language models. <i>ArXiv</i> , abs/2306.13549.	
	Pan Zhang, Xiao wen Dong, Yuhang Zang, Yuhang Cao, Rui Qian, Lin Chen, Qipeng Guo, Haodong Duan, Bin Wang, Linke Ouyang, Songyang Zhang, Wenwei Zhang, Yining Li, Yang Gao, Peng Sun, Xinyue Zhang, Wei Li, Jingwen Li, Wenhai Wang, Hang Yan, Conghui He, Xingcheng Zhang, Kai Chen, Jifeng Dai, Yu Qiao, Dahua Lin, and Jiaqi Wang. 2024. Internlm-xcomposer-2.5: A versatile large vision language model supporting long-contextual input and output. <i>ArXiv</i> , abs/2407.03320.	
	Xingcheng Zhou, Mingyu Liu, Ekim Yurtsever, Bare Luka Žagar, Walter Zimmer, Hu Cao, and Alois C. Knoll. 2023. Vision language models in autonomous driving: A survey and outlook. <i>IEEE Transactions on Intelligent Vehicles</i> .	

A Appendix: Detailed Related Work

Vision Large Language Models. Vision Large Language Models (VLLM), as one the most capable and popular solutions to multimodal tasks, extends the reasoning and generating ability of Large Language Model (LLM) beyond language modalities such as image, video, and audio (McKinzie et al., 2024b; Tong et al., 2024; Xue et al., 2024). VLLM according to their architecture (Liu et al., 2023b; Driess et al., 2023; fuy; Team, 2024). The encoder-decoder VLLM introduces additional multimodal encoders and a modality connector to project multimodal features into the spaces of

language models. The implementations of modality connector include: the projector that directly maps features into language model (Liu et al., 2024, 2023a,b); the resampler that compresses the visual feature and inserts cross-gated attention layers into the LLM decoder (Alayrac et al., 2022; Awadalla et al., 2023; Li et al., 2023a). This study mainly focuses on the LLaVA-style VLLM, which adopts encoder-decoder architecture with a projector connector.

High resolution VLLM The high-resolution problem of VLLM is attracting attention because of its prevalence in downstream tasks, such as OCR and document analysis. However, it remains challenging because high-resolution images are underrepresented in the training data, making it difficult to generalize for popular MLLMs. High-resolution VLLM solutions can be roughly divided into two classes: (1) using high-resolution vision encoders that directly support high-resolution input (Hong et al., 2023; Li et al., 2024b; Lv et al., 2023; Wei et al., 2023); (2) the patchification that cuts the high-resolution image into smaller patches to be processed on standard vision encoders (wen Dong et al., 2024; Hu et al., 2024; Feng et al., 2023; Li et al., 2023d; Xu et al., 2024). However, these solutions lack the flexibility for different resolution inputs, which can be computationally expensive. To solve this, FlexAttention uses dual tokenization that only processes a few highly-attended high-resolution tokens in the deeper LLM layers, achieving near 40% reduction in computational cost compared to standard LLaVA (Li et al., 2024a). NVLM (Dai et al., 2024) introduces 1-D tile-tagging for tile-based dynamic high-resolution images, which can significantly improve the performance of OCR-related tasks, but sometimes undermine the accuracy of reasoning-related tasks. Unlike these methods, which presuppose a fixed resolution for downstream applications, our approach implements a task-wise resolution adaptation strategy, employing different resolutions for tasks with different perceptual demands. Additionally, we enhance image input resolution through a parameter-efficient post-training method, circumventing the need for training from scratch to minimize costs.

B More Implementation Details

B.1 Vision-Language Tasks

Science-QA (Lu et al., 2022), a multimodal science question answering benchmark featuring over

21k multiple-choice questions on diverse topics. The visual component includes natural images and diagrams, testing the model’s ability to integrate both textual and visual information for coherent reasoning and explanation generation. *Vizwiz* (Gurari et al., 2018), a dataset derived from real-world images paired with spoken questions from visually impaired individuals. This task assesses a model’s ability to process low-quality, unstructured images and generate accurate responses to conversational queries. *VQAv2* (Goyal et al., 2017), an expanded version of the original Visual Question Answering (VQA) dataset, designed to reduce language biases. It challenges models to deeply understand visual content in order to answer questions about pairs of semantically similar yet visually distinct images. *TextVQA* (Singh et al., 2019), a dataset focusing on a model’s capacity to read and reason about textual elements in images, evaluating its ability to integrate Optical Character Recognition (OCR) with visual reasoning to answer questions. *OKVQA* (Marino et al., 2019), a benchmark that requires models to leverage external knowledge beyond image and question analysis, necessitating access to and reasoning with unstructured knowledge sources for accurate answers. *GQA* (Hudson and Manning, 2019), a dataset designed for real-world visual reasoning and compositional question answering, requiring models to demonstrate strong multi-modal understanding, logical reasoning, and the ability to answer questions that necessitate connecting information across both visual and linguistic domains. *MMBench* (Liu et al., 2023c), a comprehensive multimodal evaluation set with over 2,974 multiple-choice questions across 20 ability dimensions, providing a robust assessment of various vision-language skills, such as reasoning, comprehension, and explanation generation. *MMBench-CN*, a variant of MMBench focusing on tasks involving Chinese text and images, evaluating the model’s proficiency in processing and understanding multilingual data.

B.2 Baseline Methods

In addition to the original LLaVA model, we compare our method with several state-of-the-art approaches, including BLIP-2 (Li et al., 2023c), InstructBLIP (Dai et al., 2024) (with LLM backbones at two scales), Shikra (Chen et al., 2023), and IDEFICS (IDEFICS, 2023) (also with LLM backbones at two scales), as well as Qwen-VL and Qwen-VL-Chat (Bai et al., 2023). The results for

these baseline methods, along with LLaVA with the Vicuna-13B backbone, are cited from previous work (Liu et al., 2023a). For LLaVA with a Vicuna-7B backbone, we report our reproduced results across different vision-language tasks.

As a training-free baseline to extend the image input resolution, we apply positional embedding interpolation to extend the position embeddings of the vision encoder in LLaVA. This technique, widely used for Vision Transformers in VLLMs (Bai et al., 2023; Li et al., 2023b), allows models to handle higher image input resolutions than their original training resolution. We evaluate the performance of this extension without any additional training of the projector and the LLM backbone.

B.3 Method details

Image Complexity Heuristic Approach Image complexity for vision-language tasks is calculated using an open-source tool². We utilize the author-recommended hyperparameters: the number of clusters is set to 8, and the subsample rate is 0.8. To reduce computational overhead, the input image resolution is set to 112×112 , and two cluster levels are used, with their combined scores yielding the final complexity value. The complexity scores are normalized via min-max scaling, where the minimum and maximum values are computed from 100 sampled images from the ImageNet dataset (Deng et al., 2009).

RandAugment Perturbation on Image Input When assessing model variance across different resolutions, we apply random perturbations to each input image using the RandAugment algorithm, implemented via an existing tool³. For each image, we perform three random augmentations. To mitigate the effects of randomness and enhance result stability, we repeat the variance measurement process three times, each using a different random seed. The final uncertainty variance is obtained by averaging the results from these three iterations.

B.4 More Parameter-Efficient Fine-Tuning Details

The standard training hyperparameters are largely preserved, as outlined in Table 5, with two notable adjustments for image resolutions of 560^2 and 672^2 : (1) The learning rate is reduced from $2e - 5$

²https://github.com/Lou1sM/meaningful_image_complexity

³<https://github.com/TorchSSL/TorchSSL/blob/main/datasets/augmentation/randaugment.py>

Table 5: Hyperparameters at two training stages

Hyperparameter	batch size	lr	lr schedule	weight decay	epoch	optimizer	max tokens
Stage 1	256	$1e-3$	cosine decay	0	1	AdamW	2048
Stage 2	128	$2e-4$					

Table 6: Training time cost

Resolution	224×224	336×336	448×448	560×560	672×672
Training Time Cost	11h 50m	16h 17m	24h 7m	32h 29min	124h 44m

to $1e-5$ to prevent training loss explosion observed with the original rate. (2) The maximum number of tokens is increased from 2048 to 3072 and 4096, respectively, to accommodate the increased number of image tokens.

Post-training experiments are conducted on eight NVIDIA GeForce RTX 4090 GPUs, with training time costs detailed in Table 6. Due to GPU memory limitations, DeepSpeed ZeRO-3 was employed for training at the resolution of 672^2 , while ZeRO-2 was used for other resolutions. This accounts for the significant increase in training time between 672^2 and 560^2 .

In the ablation study (Section 4.4), we separately fine-tune only the projector and only the position embeddings, using the stage 1 setting for consistency with the goals of the different training stages. The corresponding hyperparameters are also detailed in Table 5.

C Impact of Statistical Distributions on Empirical Formula Performance

To evaluate the extent to which the statistical distributions of complexity $C(T)$ and uncertainty variance $V(T)$ influence the performance of the empirical formula, we present the standard deviations of $C(T)$ and $V(T)$ for each vision-language task, along with their respective ratios to the mean values. These statistics are detailed in Table 7.

The results indicate that $C(T)$ exhibits relatively low variance across tasks, whereas $V(T)$ shows substantially higher variability. This observation justifies our decision to adopt task-wise selection instead of sample-wise selection, as the higher variability in $V(T)$ at the sample level complicates consistent prediction.

To further assess the influence of $C(T)$ and $V(T)$ variance on the effectiveness of the empirical formula, we conducted an additional experiment. Specifically, we randomly sampled subsets of varying proportions from the original dataset and computed the average $C(T)$ and $V(T)$ values for these

Table 7: Statistical characteristics of $C(T)$ and $V(T)$ in each task. SD represents Standard Deviation, and Ratio indicates the ratio of the standard deviation to the mean.

Task	$C(T)$ SD	$C(T)$ Ratio	$V(T)$ SD	$V(T)$ Ratio
ScienceQA-IMG	3.3633	0.2384	0.4398	2.5466
Vizwiz	2.4405	0.1541	0.3383	6.0196
VQAv2	2.2005	0.1242	0.7925	4.2562
GQA	1.6582	0.0910	1.2595	4.9103
TextVQA	2.3057	0.1318	0.5258	3.3405
OKVQA	2.1958	0.1224	0.5487	3.7711
MMBench	3.5426	0.2196	1.2040	2.8915
MMBench-CN	3.5482	0.2197	1.0840	2.8310

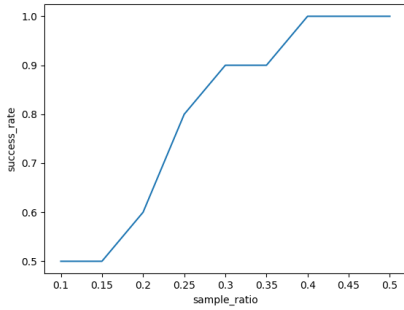


Figure 5: Relationship between sampling ratio and the success rate of the empirical formula.

subsets to estimate task-level statistics. We then evaluated the empirical formula, previously tuned using a hyperparameter k on three reference tasks, to predict the optimal resolution across all tasks under these conditions.

The sampling proportions vary from 10% to 50%, with each experiment repeated 10 times using different random seeds. The success rate was defined as the percentage of instances where the empirical formula accurately predicted the optimal resolution for all tasks. The results, presented in Figure 5, reveal the following key findings: (1) At a sampling ratio of 40%, the success rate reaches 100%, demonstrating the empirical formula’s robustness in predicting the optimal resolution. (2) At a sampling ratio of 10%, the success rate drops to 50%, indicating that a smaller subset size introduces variability that adversely affects prediction accuracy.

These findings highlight that while reducing the dataset size can lower computational costs, excessively small subsets may lead to suboptimal predictions. Moreover, the current approach relies

on random sampling; future exploration of more advanced sampling strategies that select representative samples could potentially achieve high success rates with smaller subsets.

D Reference Tasks

We utilize three reference tasks to determine the hyperparameter in Equation 3. Figure 6 presents three image samples from each reference task.

E Case Study

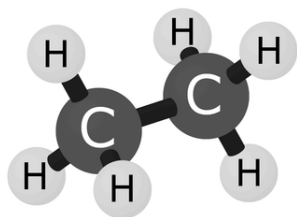
Table 8 and Table 9 demonstrate two case studies, illustrating the impact of image complexity and uncertainty variance on the performance of VLLMs. The two selected examples are drawn from the GQA dataset (Hudson and Manning, 2019).

Image Question	Figure 7a	Figure 7b
Prediction(336×336)	woman	umpire
Correct Answer	woman	batter
Image Complexity	11.35	20.62

Table 8: Same question with images in different complexity levels.

Image Question	Figure 7c	
	What is the sheet made of?	Are there stoves near the freezer to the right of the tap?
Prediction(336×336)	plastic	NO
Prediction(448×448)	plastic	YES
Correct Answer	plastic	YES
Uncertainty Variance	0.42%	16.51%

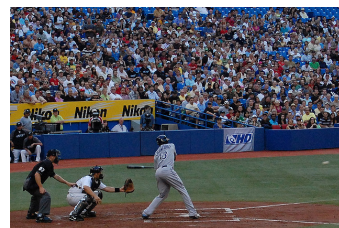
Table 9: Same image with questions in different difficulty levels.



(a) Single and simple object: Ethane is (). A. an elementary substance B. a compound



(b) Middle-level complexity: Are all the animals the same?



(c) Multiple objects: What is the brand being advertised?



(a)



(b)



(c)

Figure 7: Three case study images

F Acknowledgment of AI Assistance in Writing and Revision

We utilized LLMs for revising and enhancing writing of this paper.